# Electric potential and Fréchet derivatives for a uniform anisotropic medium with a tilted axis of symmetry

**Journal Article**

**Author(s):**
Greenhalgh, S. A.; Marescot, L; Zhou, B.; Greenhalgh, M.; Wiese, T.

# Electric Potential and Fréchet Derivatives for a Uniform Anisotropic Medium with a Tilted Axis of Symmetry

S. A. Greenhalgh,[1,2] L. Marescot,[2] B. Zhou,[1] M. Greenhalgh,[1] and T. Wiese[1]

*Abstract*—In this paper we develop analytic solutions for the electric potential, current density and Fréchet derivatives at any interior point within a 3-D transversely isotropic medium having a tilted axis of symmetry. The current electrode is assumed to be on the surface of the Earth and the plane of stratification given arbitrary strike and dip. Profiles can be computed for any azimuth. The equipotentials exhibit an elliptical pattern and are not orthogonal to the current density vectors, which are strongly angle dependent. Current density reaches its maximum value in a direction parallel to the longitudinal conductivity direction. Illustrative examples of the Fréchet derivatives are given for the 2.5-D problem, in which the profile is taken perpendicular to strike. All three derivatives of the Green's function with respect to longitudinal conductivity, transverse resistivity and dip angle of the symmetry axis ($dG/d\sigma_l$, $dG/d\sigma_t$, $dG/d\theta_0$) show a strongly asymmetric pattern compared to the isotropic case. The patterns are aligned in the direction of the tilt angle. Such sensitivity patterns are useful in real-time experimental design as well as in the fast inversion of resistivity data collected over an anisotropic earth.

Key words: Resistivity, anisotropy, electric potential, Fréchet, sensitivity.

## 1. Introduction

In a recent paper we presented a general formulation for calculating the electric potential and Fréchet derivatives in an arbitrary 3-D anisotropic, heterogeneous medium (Greenhalgh *et al*., 2008a). It was based on a new Gaussian quadrature grid formulation for calculating the 3-D Green's functions.

In this paper we develop an analytic solution to the problem for a surface current source above an otherwise homogeneous but anisotropic medium. We take the special case of a transversely isotropic medium with a tilted axis of symmetry (TTI medium), such as might occur for dipping beds, inclined fractures, oriented cleavage, foliation and other stratifications. We derive in an alternative fashion the basic equations for the voltage, the current density and the sensitivity functions at an arbitrary interior point in the medium. The analytic solutions can be a useful check on numerical

modelling code. They can also be incorporated into a fast imaging method. For example, LOKE and BARKER (1995) used a uniform isotropic model to deconvolve resistivity data for effects of the electrode array. ZHOU and GREENHALGH (2002) gave a more elaborate treatment referred to as the analytic sensitivity function to produce an initial model far superior to a pseudo-section, and which considers array effects. It is somewhat akin to a seismic migration. However to date, such a fast electrical imaging approach has not been done for anisotropic models. The sensitivity functions (Fréchet derivatives) are particularly important in optimised experimental design (STUMMER *et al.*, 2004) and in actual inversion of resistivity data (ZHOU and GREENHALGH, 1999). Few papers in the resistivity modelling and inversion literature incorporate anisotropy (DAS, 1995; YIN and WIEDELT, 1999; PAIN *et al.*, 2003, HERWANGER *et al.*, 2004; LI and SPITZER, 2005; KIM *et al*., 2006; ZHOU *et al.,* 2009). They offer purely numerical solutions—mainly finite element and finite difference—for the potential in general inhomogeneous media.

An analytic solution for the potential on the *surface* of a uniform TTI medium was given by ASTEN (1974) and BHATTACHARYA and PATRA (1968). Several authors have extended the treatment for an anisotropic half space. The integral equation approach was used by PAL and DASGUPTA (1984) to derive the electric potential due to a surface point source over an inhomogeneous, anisotropic half space of the simple vertical transversely isotropic (VTI) type. A modification of this was made by PAL and MUKHERJEE (1986) who dealt with a layered conducting earth with dipping anisotropy. WAIT (1982, 1990) considered 3-D current flow into a single or two layer anisotropic half space, but took the coordinate axes to coincide with the principal conductivity directions. ELORANTA (1988) modelled *mise à la masse* anomalies in a transversely isotropic medium containing prismatic conductors, while ESKOLA and HONGISTO (1997) considered an anisotropic body located in an isotropic environment. FLYKT *et al.* (1996) calculated the electric potential anomalies caused by a conducting body in an anisotropic conducting half space. LI and UREN (1997) gave analytic solutions for the point source potential in an anisotropic 3-D half space, comprising either two horizontal layers or two vertical boundary planes. In another paper (LI and UREN, 1998) they applied image theory to derive the solution for the potential from a *buried* current source in an arbitrary anisotropic half space, and showed how the image source is laterally displaced from the true source horizontal position. LI and STAGNITTI (2000) studied the problem of direct current electric potential in an anisotropic halfspace with a vertical contact and containing a conductive 3-D body. The analytic solution for the potential in a stack of layers, each having arbitrary anisotropy, was derived by PERVAGO *et al*. (2006) by applying a set of Hankel transforms of integer order. None of the above papers offer a formulation for the Fréchet derivatives. To the best of our knowledge this is the first time that the sensitivities of the potential to the anisotropic parameters for a homogeneous TTI medium have been formally investigated.

## 2. The Conductivity Tensor

The conductivity tensor $\boldsymbol{\sigma}$, which relates the current density $\mathbf{J}$ to the electric field $\mathbf{E}$ (or potential gradient $-\nabla U$) through the Ohm's Law relation:

$$J_i = \sigma_{ij}E_j \quad i,j = x,y,z \tag{1}$$

is of rank 2 and for the most general anisotropic medium can be described by six independent components. Writing it out as a $3 \times 3$ symmetric matrix in the Cartesian coordinate or recording frame, we have:

$$\boldsymbol{\sigma} = \begin{pmatrix} \sigma_{xx} & \sigma_{xy} & \sigma_{xz} \\ \sigma_{xy} & \sigma_{yy} & \sigma_{yz} \\ \sigma_{xz} & \sigma_{yz} & \sigma_{zz} \end{pmatrix} \tag{2}$$

The matrix can be diagonalised to produce the three eigenvalues $\sigma_1$, $\sigma_2$, $\sigma_3$ which yield the principal conductivities in the directions of the three principal axes or eigenvectors $\hat{\mathbf{x}}'$, $\hat{\mathbf{y}}'$, $\hat{\mathbf{z}}'$:

$$\boldsymbol{\sigma}' = \begin{pmatrix} \sigma_{x'x'} & 0 & 0 \\ 0 & \sigma_{y'y'} & 0 \\ 0 & 0 & \sigma_{z'z'} \end{pmatrix} = \begin{pmatrix} \sigma_1 & 0 & 0 \\ 0 & \sigma_2 & 0 \\ 0 & 0 & \sigma_3 \end{pmatrix}. \tag{3}$$

The eigenvectors are all orthogonal. These directions refer to the natural frame of the rock and reflect the symmetry axes or the actual rock structure/fabric. In these directions, $\mathbf{J}$ is parallel to $\mathbf{E}$, but for all other directions, the current density and electric field are in different directions to each other. The three Euler angles, which permit a rotation from the Cartesian frame into the principal directions, together with the three eigenvalues, constitute an alternative set of the six independent components of the tensor to those given by equation (2).

For second rank symmetric tensors like the conductivity tensor, there is a simple geometrical representation referred to as the representation quadric (NYE, 1957):

$$\sigma_{ij}x_ix_j = 1 \tag{4}$$

or expanding out into the various components:

$$\sigma_{xx}x^2 + \sigma_{yy}y^2 + \sigma_{zz}z^2 + 2\sigma_{xy}xy + 2\sigma_{xz}xz + 2\sigma_{yz}yz = 1. \tag{5}$$

This is the equation of an ellipsoid, centred at the origin, in the Cartesian coordinate frame. The axes of the ellipsoid are tilted in the directions of the principal directions mentioned above (see Fig. 1a). By a co-ordinate rotation, the cross terms (or off-diagonal elements) in the above equation are eliminated yielding, in the natural rock frame $x'$, $y'$, $z'$:

$$\sigma_1 x^{'2} + \sigma_2 y^{'2} + \sigma_3 z^{'2} = 1. \tag{6}$$

**(a)**    Geographic frame



**(b)**    Principal axis frame



$$a = \frac{1}{\sqrt{\sigma_1}} \qquad b = \frac{1}{\sqrt{\sigma_2}} \qquad c = \frac{1}{\sqrt{\sigma_3}}$$
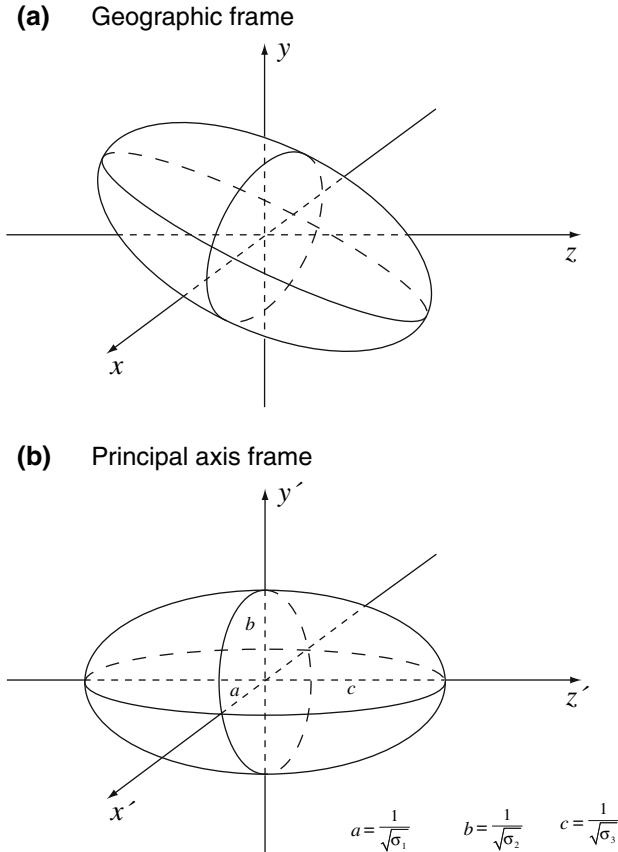
Figure 1

The conductivity tensor ellipsoid in (a) the geographic co-ordinate frame $x$, $y$, $z$, and (b) in the principal axis frame (or natural rock frame) $x'$, $y'$, $z'$. The lengths of the semi major axes are equal to the inverse square roots of the principal conductivities (or eigenvalues of the $3 \times 3$ conductivity matrix). The directions of the principal axes are the corresponding eigenvectors.

The semi–major axis lengths of the ellipsoid are equal to the inverse of the square roots of the eigenvalues or principal conductivities (see Fig. 1b). If we choose to work with the resistivity tensor, which is the inverse of the conductivity, $\boldsymbol{\rho} = \boldsymbol{\sigma}^{-1}$, then the semi-axes are equal in length to the square roots of the principal resistivities using the relations:

$$\rho_1 = 1/\sigma, \ \rho_2 = 1/\sigma_2, \ \rho_3 = 1/\sigma_3$$

For an electric field oriented in an arbitrary direction $\hat{\mathbf{n}}$ from the centre of the ellipsoid to the surface of the ellipsoid, the radius $r$ (or distance along this line) gives the square root of the resistivity in that direction (see Fig. 2). The normal to the tangent at $P$ gives the direction of the current density vector (Fig. 2). Obviously, for an isotropic medium
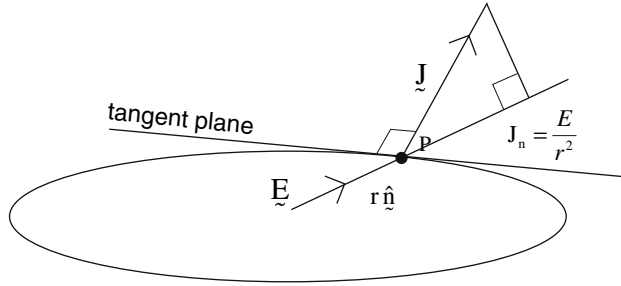
Figure 2
Diagram showing the relationship between the electric field vector **E** and the current density vector **J**. The $E$ field is in direction **n** whereas the **J** vector is orthogonal to the tangent plane where the line $r\boldsymbol{n}$ meets the surface of the ellipsoid. The current density in direction **n** is simply $E/r^2$ where $r$ is length of line from the centre of the ellipsoid to its surface in direction **n.**

the ellipsoid reduces to a sphere and the radius is normal to the surface, yielding **J** parallel to **E**. The current density in the direction $\hat{\mathbf{n}}$ of the electric field is given by:

$$J_n = \mathbf{J} \cdot \hat{\mathbf{n}} = \sigma_n E = E/r^2 \tag{7}$$

with $E$ being the magnitude of vector **E**, $r$ the length from the centre of the ellipsoid to the point on its surface intersected by the **E** vector and $\sigma_n$ is the conductivity in direction $\hat{\mathbf{n}}$, given by:

$$\sigma_n = \sigma_{ij} n_i n_j. \tag{8}$$

Summation is implied by the repeated subscripts and the unit vector $\hat{n}$ is found from:

$$\hat{\mathbf{n}} = \mathbf{E}/E.$$

The long axis of the conductivity ellipsoid $\hat{\mathbf{z}}'$, which represents the direction of the dominant principal resistivity, often coincides with the normal to the major rock foliation. It is referred to as the transverse direction. It is characterised by polar angles $\theta_0$ and $\phi_0$, which give the inclination and azimuth respectively in spherical coordinates. It has components:

$$\hat{\mathbf{z}}' = (\cos \phi_0 \sin \theta_0, \sin \theta_0 \sin \phi_0, \cos \phi_0). \tag{9}$$

The other two principal directions lie in the plane perpendicular to this direction. The third angle required to characterise the principal directions is the azimuth swing (call it $\varepsilon$) of $\hat{\mathbf{x}}'$ from that of $\hat{\mathbf{z}}'$. The orthogonality property defines the third vector uniquely. A special case is that in which $\varepsilon = 0$ so that direction $\hat{\mathbf{x}}'$ is obtained simply by adding 90 degrees to $\theta$:

$$\hat{\mathbf{x}}' = (\cos \phi_0 \cos \theta_0, \sin \phi_0 \cos \theta_0, -\sin \theta_0). \tag{10}$$

The third unit vector $\hat{\mathbf{y}}'$ is obtained by taking the cross-product:

$$\hat{\mathbf{y}}' = \hat{\mathbf{z}}' \times \hat{\mathbf{x}}' = (-\sin\phi_0, \ \cos\phi_0, \ 0). \tag{11}$$

So defining as the rotation matrix:

$$\mathbf{R} = \begin{pmatrix} \hat{\mathbf{x}}' \\ \hat{\mathbf{y}}' \\ \hat{\mathbf{z}}' \end{pmatrix} = \begin{pmatrix} \cos\phi_0 \cos\theta_0, & \sin\phi_0 \cos\theta_0, & -\sin\theta_0 \\ -\sin\phi_0, & \cos\phi_0, & 0 \\ \cos\phi_0 \sin\theta_0, & \sin\phi_0 \sin\theta_0, & \cos\theta_0 \end{pmatrix} \tag{12a}$$

we can now compute the conductivity matrix in the Cartesian or recording frame as the product of the three matrices:

$$\boldsymbol{\sigma} = \mathbf{R}^{\mathbf{T}}\boldsymbol{\sigma}'\mathbf{R}, \tag{12b}$$

where the diagonal eigenvalue matrix $\boldsymbol{\sigma}'$ is given by equation (3). The same rotation matrix R obtains for the resistivity tensor $\boldsymbol{\rho}$. The six components of the conductivity tensor can now be written out as follows in terms of the principal conductivities and the two polar angles defining the direction of the dominant eigenvector (note that the following expression is not implied to be a vector, but merely a list of components):

$$\begin{pmatrix} \sigma_{xx} \\ \sigma_{xy} \\ \sigma_{xz} \\ \sigma_{yy} \\ \sigma_{yz} \\ \sigma_{zz} \end{pmatrix} = \begin{pmatrix} \sigma_1 \cos^2\theta_0 \cos^2\phi_0 + \sigma_2 \sin^2\phi_0 + \sigma_3 \sin^2\theta_0 \cos^2\phi_0 \\ 0.5(\sigma_1 \cos^2\theta_0 \sin 2\phi_0 - \sigma_2 \sin 2\phi_0 + \sigma_3 \sin^2\theta_0 \sin 2\phi_0) \\ 0.5(-\sigma_1 + \sigma_3)\cos\phi_0 \sin 2\theta_0 \\ \sigma_1 \cos^2\theta_0 \sin^2\phi_0 + \sigma_2 \cos^2\phi_0 + \sigma_3 \sin^2\theta_0 \sin^2\phi_0 \\ 0.5(-\sigma_1 + \sigma_3)\sin\phi_0 \sin 2\theta_0 \\ \sigma_1 \sin^2\theta_0 + \sigma_3 \cos^2\theta_0 \end{pmatrix}. \tag{13}$$

The 2.5-D case, with one principal axis along the strike or $y$ direction (i.e., $y$ is parallel to $y'$) is obtained by letting the azimuth angle $\phi_0 = 0$ in the above equation, which gives:

$$\begin{pmatrix} \sigma_{xx} \\ \sigma_{yy} \\ \sigma_{xz} \\ \sigma_{zz} \end{pmatrix} = \begin{pmatrix} \sigma_1 \cos^2\theta_0 + \sigma_3 \sin^2\theta_0 \\ \sigma_2 \\ 0.5(-\sigma_1 + \sigma_3)\sin 2\theta_0 \\ \sigma_1 \sin^2\theta_0 + \sigma_3 \cos^2\theta_0 \end{pmatrix}. \tag{14}$$

Note that in both cases, the trace of the $\sigma$ matrix ($=\sigma_{xx} + \sigma_{yy} + \sigma_{zz}$) is equal to the sum of the eigenvalues $\sigma_1 + \sigma_2 + \sigma_3$.

### 2.1. *The TTI Case*

A special case for the 3-D situation where azimuth is still important is that in which the two principal conductivities in the plane perpendicular to $\hat{\mathbf{z}}'$ are equal. i.e., eigenvalues $\sigma_1 = \sigma_2$.

This is referred to as a tilted transversely isotropic (TTI) medium. The medium anisotropy is then characterised by just four parameters: the longitudinal and transverse resistivities ($\rho_l = 1/\sigma_1 = 1/\sigma_2$ and $\rho_t = 1/\sigma_3$, the so-called principal resistivites) and the two polar angles, dip $\theta_0$ and azimuth $\phi_0$ which define the arbitrary axis of symmetry which lies normal to the plane of stratification (e.g., bedding plane, fracture plane, cleavage plane). This plane is characterised in terms of strike angle $\beta(=\phi_0 + 90)$ degrees and dip angle from the horizontal $\alpha = \theta_0$ (see Fig. 3). Resistivity is constant at $\rho_l$ for any direction within the bedding plane, although different in all other directions, reaching its maximum value $\rho_t$ along the symmetry axis or so-called transverse direction ($\phi_0, \theta_0$). The tensor ellipsoid for this special case of TI media has a circular cross section perpendicular to the long axis.

As an alternative to $\rho_l$, and $\rho_t$, we can introduce two auxiliary quantities:

$$\rho_m = \sqrt{\rho_l \rho_t}$$
$$\lambda = \sqrt{\frac{\rho_t}{\rho_l}} \quad . \tag{15}$$

The quantity $\lambda$ is called the coefficient of anisotropy, typically ranging 1 to 3 (KELLER and FRISCHKNECHT, 1970), while $\rho_m$ is the geometric mean of the two principal resistivities $\rho_l$, $\rho_t$. It is sometimes referred to as the equivalent isotropic medium resistivity value.
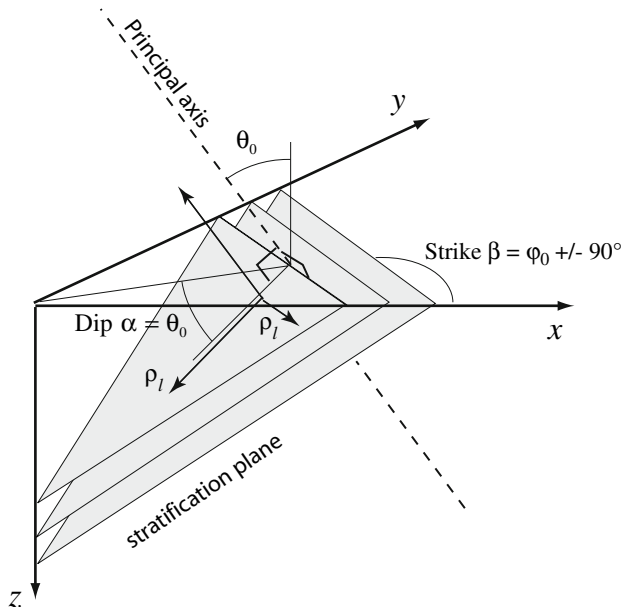


Figure 3

Plane of stratification (bedding plane, fracture plane) having strike $\beta$ and dip (from horizontal) of $\alpha$. The longitudinal resistivity is $\rho_l$ in the plane of the bedding and the transverse resistivity is $\rho_t$ in the direction of the normal to the bedding plane, defined by the polar angles $\phi_o$, $\theta_0$.

Using the simplified form of equation (13) for the tilted TI medium in which $\sigma_1 = \sigma_2 = \sigma_l$ and $\sigma_3 = \sigma_t$ then the elements of the conductivity tensor reduce to the following (again, it is merely a list, a vector is not implied by bracketing the quantities):

$$\begin{pmatrix} \sigma_{xx} \\ \sigma_{xy} \\ \sigma_{xz} \\ \sigma_{yy} \\ \sigma_{yz} \\ \sigma_{zz} \end{pmatrix} = \begin{pmatrix} \sigma_l \cos^2 \theta_0 \cos^2 \phi_0 + \sigma_l \sin^2 \phi_0 + \sigma_t \sin^2 \theta_0 \cos^2 \phi_0 \\ 0.5(-\sigma_l + \sigma_t) \sin^2 \theta_0 \sin 2\phi_0 \\ 0.5(-\sigma_l + \sigma_t) \cos \phi_0 \sin 2\theta_0 \\ (-\sigma_l + \sigma_t) \sin^2 \theta_0 \sin^2 \phi_0 + \sigma_l \\ 0.5(-\sigma_l + \sigma_t) \sin \phi_0 \sin 2\theta_0 \\ \sigma_l \sin^2 \theta_0 + \sigma_t \cos^2 \theta_0 \end{pmatrix}. \tag{16}$$

As a check, we see that in the isotropic case if $\sigma_l = \sigma_t = \sigma$ then all diagonal elements $\sigma_{ii}$ of the tensor reduce to the same scalar value $\sigma$, whereas the off-diagonal elements all go to zero.

For the general 2.5-D case with no azimuthal dependence, we obtain:

$$\begin{pmatrix} \sigma_{xx} \\ \sigma_{yy} \\ \sigma_{xz} \\ \sigma_{zz} \end{pmatrix} = \begin{pmatrix} \sigma_l \cos^2 \theta_0 + \sigma_t \sin^2 \theta_0 \\ \sigma_l \\ 0.5(-\sigma_l + \sigma_t) \sin 2\theta_0 \\ \sigma_l \sin^2 \theta_0 + \sigma_t \cos^2 \theta_0 \end{pmatrix}. \tag{17}$$

## 3. Potential and Current Density within a Tilted TI Medium

### 3.1. VTI Medium

KELLER and FRISCHKNECHT (1970) show for a medium having a vertical symmetry axis (i.e., horizontally layered or VTI medium) the potential $U$ at some arbitrary point P($x$, $y$, $z$) in the medium due to a current source $I$ on the surface at the origin is given by:

$$U(x, y, z) = \frac{I \rho_l \lambda}{2\pi (x^2 + y^2 + \lambda^2 z^2)^{1/2}}. \tag{18a}$$

The equipotential surfaces are then given by:

$$x^2 + y^2 + \lambda^2 z^2 = C \tag{18b}$$

where $C$ is a constant. i.e., they are ellipsoids of revolution about the z-axis. The components of the current density vector **J** are given by:

$$J_x = \frac{-1}{\rho_l}\frac{\partial U}{\partial x}$$
$$J_y = \frac{-1}{\rho_l}\frac{\partial U}{\partial y}. \tag{19}$$
$$J_z = \frac{-1}{\rho_t}\frac{\partial U}{\partial z}$$

Now we can recast these results entirely in terms of the distance $R = \sqrt{x^2 + y^2 + z^2}$ to the point of measurement and the angle of inclination $\psi$ from the symmetry axis (in this special case it is vertical) using:

$$\begin{aligned} x^2 + y^2 &= R^2 \sin^2 \psi \\ z^2 &= R^2 \cos^2 \psi \end{aligned}. \tag{20}$$

Note that for a vertical axis of symmetry the situation is axi-symmetric, i.e., has azimuthal symmetry. Therefore there is no dependence of the potential on the azimuth angle to the point P.

Therefore

$$U = \frac{I\lambda\rho_l}{2\pi R(1 + (\lambda^2 - 1)\cos^2\psi)^{1/2}}. \tag{21}$$

Differentiating this expression and substituting into (19) enables computation of the components of the current density in terms of the new coordinates. The component of current density in the parallel direction of the symmetry axis ($J_{par} = J_z$) is given by:

$$J_{par} = \frac{\lambda I \cos\psi}{2\pi R^2 (1 + (\lambda^2 - 1)\cos^2\psi)^{3/2}} \tag{22}$$

and that in the orthogonal direction $J_{perp}\left(= \sqrt{J_x^2 + J_y^2}\right)$ is given by:

$$J_{perp} = \frac{\lambda I \sin\psi}{2\pi R^2 (1 + (\lambda^2 - 1)\cos^2\psi)^{3/2}}. \tag{23}$$

### 3.2. TTI Medium

Now we want to translate these results into situations where the axis of symmetry is tilted in some arbitrary direction. For such a TTI medium let the axis of symmetry have azimuth $\phi_0$ (from the x axis) and inclination angle (from the vertical or z axis) of $\theta_0$ (see Fig. 4). The unit vector $\hat{\mathbf{z}}'$ defining this direction has Cartesian components given by equation (9).

The point P at which we want to compute the potential and the current density can be defined in spherical coordinates $(R, \phi, \theta)$. The unit vector defining this direction has Cartesian components:
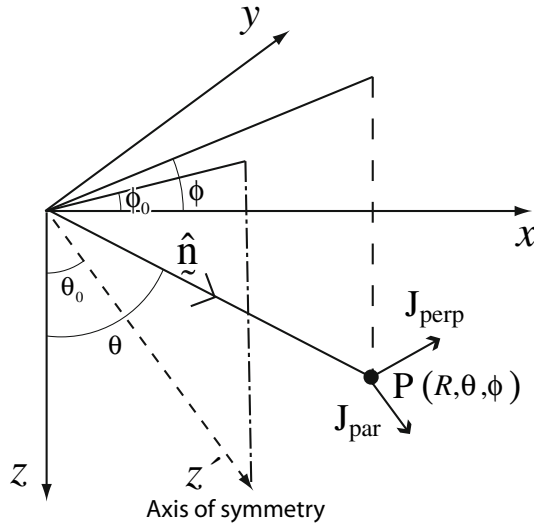
Figure 4

Point P(R, $\phi$, $\theta$) inside an anisotropic medium having tilted axis of symmetry (defined by angles $\phi_0$, $\theta$) at which potential $U$ and current density *J* are to be computed.

$$\hat{\mathbf{n}} = (\sin\theta\cos\phi, \sin\theta\sin\phi, \cos\theta). \tag{24}$$

The cosine of the incident angle $\psi$ measured relative to the symmetry axis is found by taking the dot product between the unit vectors $\hat{\mathbf{z}}'$ and $\hat{\mathbf{n}}$:

$$\cos\psi = \hat{\mathbf{z}}' \cdot \hat{\mathbf{n}} = \sin\theta_0 \cdot \sin\theta \cdot \cos(\phi - \phi_0) + \cos\theta_0\cos\theta. \tag{25}$$

If we now substitute for cos $\psi$ from equation (25) into equation (21) we find the *potential* at any interior point P(*R, $\phi$, $\theta$)* for a rotated symmetry axis, in the geographic frame. Such a construction, in going from the VTI to the TTI case, is commonplace in seismic anisotropy (see for example, ZHOU and GREENHALGH, 2004). The electric potential takes the same form in both the VTI and TTI cases but the $\psi$ angle, as given by equation (25), is different in each case. For VTI media $\theta_0 = 0$, and $\psi = \theta$.

A confirmation of the validity of equations (21) and (25) in the general TTI case can be easily established. We start with the general uniform anisotropic medium expression for the potential (see LI and UREN, 1998; LI and SPITZER, 2005):

$$U = \frac{C}{\sqrt{\mathbf{r}^T \cdot \boldsymbol{\rho} \cdot \mathbf{r}}} = \frac{C}{\sqrt{\rho_{xx}x^2 + \rho_{yy}y^2 + \rho_{zz}z^2 + 2\rho_{xy}xy + 2\rho_{xz}xz + 2\rho_{yz}yz}}, \tag{26}$$

where $\mathbf{r} = (x, y, z)$, $C$ is a constant $= I(\det \rho_{ij})^{1/2}/2\pi = I(\rho_{x'x'}\cdot\rho_{y'y'}\cdot\rho_{z'z'})^{1/2}/2\pi)$, $I$ is the strength of the current source, located at the origin, and $\boldsymbol{\rho}$ ($=[\sigma_{ij}]^{-1}$) is the resistivity tensor, the inverse matrix of the conductivity tensor. Note that the primed, subscripted

values are the principal resistivity values referred to earlier as $\rho_1$, $\rho_2$, $\rho_3$. We must now convert from Cartesian to spherical co-ordinates using:

$$
\begin{aligned}
x &= R\cos\phi\sin\theta \\
y &= R\sin\phi\sin\theta\,, \\
z &= R\cos\theta
\end{aligned}
\tag{27}
$$

and use the following expressions for the components of the resistivity tensor in a TTI medium:

$$
\begin{pmatrix} \rho_{xx} \\ \rho_{xy} \\ \rho_{xz} \\ \rho_{yy} \\ \rho_{yz} \\ \rho_{zz} \end{pmatrix}
=
\begin{pmatrix}
\rho_l\cos^2\theta_0\cos^2\phi_0 + \rho_l\sin^2\phi_0 + \rho_t\sin^2\theta_0\cos^2\phi_0 \\
0.5(\rho_t - \rho_l)\sin^2\theta_0\sin 2\phi_0 \\
0.5(\rho_t - \rho_l)\cos\phi_0\sin 2\theta_0 \\
(\rho_t - \rho_l)\sin^2\theta_0\sin^2\phi_0 + \rho_l \\
0.5(\rho_t - \rho_l)\sin\phi_0\sin 2\theta_0 \\
\rho_l\sin^2\theta_0 + \rho_t\cos^2\theta_0
\end{pmatrix},
\tag{28}
$$

These components are simply obtained by inverting the conductivity matrix (see equation (16) for its elements). It is obvious that the same Euler rotations are involved for the conductivity tensor and the resistivity tensor, because we obtain the elements of the resistivity matrix by replacing the principal conductivities in the conductivity matrix with the principal resistivity values. It is trivial to show that $\boldsymbol{\sigma}.\boldsymbol{\rho}$ yields the identity matrix. After substituting for all of the terms in equations (27) and (28) into equation (26), and after some algebraic and trigonometric manipulations, it reduces to the identical form of equation (21) with $\cos(\psi)$ given by equation (25).

In similar fashion as we did for the potential, it is possible to find the ***current density J*** for a tilted axis of symmetry in terms of the original coordinate system:

$$
\begin{aligned}
J_x &= J_{par}\cos\phi_0\sin\theta_0 + J_{perp}\cos\phi_0\cos\theta_0 \\
J_y &= J_{par}\sin\phi_0\sin\theta_0 + J_{perp}\sin\phi_0\cos\theta_0 \\
J_z &= J_{par}\cos\theta_0 - J_{perp}\sin\theta_0
\end{aligned}
\tag{29}
$$

where $J_{par}$, $J_{perp}$ are given by equations (22) and (23) and are shown in Figure 4.

### 3.3. Special Cases

For a *vertical axis of symmetry* $\theta_0 = 0$ so $\cos\psi = \cos\theta$ and $\psi = \theta$ and the general solution (equation 21) reverts to the earlier expression for the VTI medium, with no azimuthal dependence:

$$
U(R, \phi, \theta) = \frac{I\rho_m}{2\pi R(1 + (\lambda^2 - 1)\cos^2\theta)^{1/2}},
\tag{30}
$$

where again $\rho_m = \lambda\rho_l$.

For vertically dipping beds, or a *horizontal axis of symmetry* $\theta_0 = 90$ we have

$$\cos \psi = \sin \theta \cos(\phi - \phi_0) \tag{31}$$

and the potential is given by:

$$U(R, \phi, \theta) = \frac{I \rho_m}{2\pi R(1 + (\lambda^2 - 1) \sin^2 \theta \cos^2(\phi - \phi_0))^{1/2}}. \tag{32}$$

Consider now a point P *on the surface* of the Earth. Here $z = 0$, or $\theta = 90$ and from equation (25):

$$\cos \psi = \sin \theta_0 \cos(\phi - \phi_0). \tag{33}$$

Substituting into equation (21) we find that the surface potential is given by:

$$U(x, y, 0) = U(r, \phi, 0) = \frac{I \rho_m}{2\pi r(1 + (\lambda^2 - 1) \cos^2(\phi - \phi_0) \sin^2 \theta_0)^{1/2}}, \tag{34}$$

where $r^2 = x^2 + y^2$.

This is the same result as that given by BHATTACHARYA and PATRA (1968, p.18), although they expressed it in terms of the bedding plane strike $\beta$ $(=\phi_0 - \phi + 90)$ and dip from the horizontal $\alpha (= \theta_0)$. They do not give expressions for potential in the subsurface.

For a vertical axis of symmetry $\theta_0 = 0$ (bedding plane dip of zero) then the potential is given by:

$$U = \frac{I \rho_m}{2\pi r} \tag{35}$$

with no azimuthal dependence. The apparent resistivity for a pole-pole array is given by:

$$\rho_a = 2\pi r \cdot \frac{U}{I} = \rho_m = \lambda \rho_l. \tag{36}$$

Note that this is the case of a profile oriented in a direction parallel to the layering or in the longitudinal resistivity direction yet the apparent resistivity is greater than the longitudinal resistivity by a factor equal to the coefficient of anisotropy.

Next consider the case of *vertically dipping beds*, i.e., horizontal axis of symmetry $\theta_0 = 90$ and again with observations at the Earth's surface. Consider a profile perpendicular to the strike of the bedding plane, $\phi = \phi_0$. From equation (34) we find that

$$U(r, \phi, 90) = \frac{I \rho_m}{2\pi r \cdot \lambda} = \frac{I \rho_l}{2\pi r} \tag{37}$$

and the apparent resistivity for a pole-pole array is $\rho_a = \rho_l$.

Note that this is the case of a profile oriented in a direction perpendicular to the layering or in the transverse resistivity direction, yet the apparent resistivity is equal to

the longitudinal resistivity, not the transverse resistivity. This is referred to as the Paradox of Anisotropy (MAILLET, 1947; BHATTACHARYA and PATRA, 1968).

For profiles parallel to the strike of the bedding plane the apparent resistivity is again equal to $\rho_m$. There is a clear azimuthal dependence in the apparent resistivity, with values ranging between $\rho_l$ and $\rho_m$.

## 4. Fréchet Derivatives

### 4.1. General case

The Fréchet derivatives relate the perturbation in the measured potential with a given electrode configuration to a perturbation in the medium properties at some subsurface position. Normally they are computed for all subsurface positions and for all electrode combinations to show the sensitivity behaviour with each configuration and facilitate updates in the conductivity estimates during a nonlinear inversion of electrical resistivity data. Using the constant block approximation for conductivity specification, GREENHALGH et al. (2008a), using a formal perturbation analysis and the self-adjoint nature of the differential operator, derived the following formula for the derivatives of the potential with respect to the model parameters $m_\beta$ in the most general 3-D anisotropic, heterogeneous medium:

$$\frac{\partial U}{\partial (m_\beta)_p} = -I w_p \left\{ \left( \frac{\partial \sigma_{ij}}{\partial m_\beta} \frac{\partial G^A}{\partial x_j} \frac{\partial G^M}{\partial x_i} \right)_p \quad m_\beta \in \sigma_{ij} \right. \tag{38}$$

or $m_\beta = (\sigma_1, \sigma_2, \sigma_3, \phi_0, \theta_0, \varepsilon)$.

Note that summation is implied through repetition of subscripts $i, j = x, y, z$.

Here $G^A$ is the Green's function for the current electrode A, and $G^M$ is the adjoint Green's function for the receiver electrode M (see Fig. 5). They have to be calculated numerically such as by a finite element or finite difference scheme. We recently presented a new Gaussian quadrature grid scheme for evaluation of the Green's functions, which enables easy incorporation of surface topography and medium anisotropy (ZHOU et al., 2009). The quantity $w_p$ appearing above is the product of the Gaussian weights (for each coordinate direction) at the Gaussian point $p$. The volume is divided into a 3-D Gaussian quadrature grid and a Gaussian quadrature formula used to calculate the volume integral arising in the weak form of solution of the partial differential equation.

The first term inside the brackets in the above expression involves the derivatives of the conductivity tensor with respect to each of the independent parameters (normally the eigenvalues or principal conductivities, and the angles defining their directions). They can be evaluated once the specific class of anisotropy is specified (see later).

Dropping the $p$ and $\beta$ subscripts, recognising the symmetry of the conductivity tensor, and omitting the current strength and Gaussian weight terms, we can write out equation (38) in full for a given model parameter $m$ in terms of all the components:
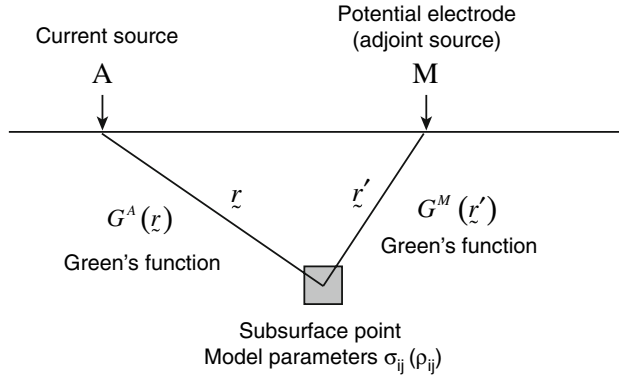
Figure 5

Arbitrary Gaussian point $p$ inside the anisotropic medium at which the Fréchet derivative is to be calculated. The Fréchet derivative depends on the two Green's functions for the true current source A and the adjoint current source (or potential electrode position) M. The conductivity tensor at this Gaussian point is $\sigma_{ij}(p)$.

$$
\begin{aligned}
-\frac{\partial U}{\partial m} = {} & \frac{\partial \sigma_{xx}}{\partial m} \cdot \frac{\partial G^A}{\partial x} \cdot \frac{\partial G^M}{\partial x} + \frac{\partial \sigma_{yy}}{\partial m} \cdot \frac{\partial G^A}{\partial y} \cdot \frac{\partial G^M}{\partial y} + \frac{\partial \sigma_{zz}}{\partial m} \cdot \frac{\partial G^A}{\partial z} \cdot \frac{\partial G^M}{\partial z} \\
& + \frac{\partial \sigma_{xy}}{\partial m} \left( \frac{\partial G^A}{\partial x} \cdot \frac{\partial G^M}{\partial y} + \frac{\partial G^A}{\partial y} \cdot \frac{\partial G^M}{\partial x} \right) \\
& + \frac{\partial \sigma_{xz}}{\partial m} \left( \frac{\partial G^A}{\partial x} \cdot \frac{\partial G^M}{\partial z} + \frac{\partial G^A}{\partial z} \cdot \frac{\partial G^M}{\partial x} \right) \\
& + \frac{\partial \sigma_{yz}}{\partial m} \left( \frac{\partial G^A}{\partial y} \cdot \frac{\partial G^M}{\partial z} + \frac{\partial G^A}{\partial z} \cdot \frac{\partial G^M}{\partial y} \right).
\end{aligned}
\tag{39}
$$

In the case of an *isotropic medium* we have:

$$
\sigma_{xx} = \sigma_{yy} = \sigma_{zz} = \sigma, \quad \sigma_{xy} = \sigma_{xz} = \sigma_{yz} = 0
\tag{40}
$$

all the cross terms above disappear, the derivatives $\frac{\partial \sigma_{ii}}{\partial m}$ all equal 1 and equation (39) reduces to:

$$
\frac{\partial U}{\partial \sigma} = -\nabla G^A . \nabla G^M
\tag{41}
$$

which apart from the constant factor $I$ (strength of current source) is the same result as obtained by ZHOU and GREENHALGH (1999).

Equations (38) and (39) are in terms of potential, and are really applicable to a pole-pole (two electrode) configuration. When working with potential difference or apparent resistivity $\rho_a$, say for three electrode or four electrode arrays, the expression can be easily modified. However, in such cases the potential for each current source (or sink) and each of the potential electrodes (adjoint sources) would have to be considered (see ZHOU and GREENHALGH, 1999 for the isotropic case expressions for $\partial \rho_a / \partial \sigma$). In fact, all electrode combinations can be synthesised from the pole–pole configuration by simple algebraic addition.

### 4.2. Uniform TTI medium

The Green's functions in the case of a uniform anisotropic medium can be calculated analytically. In earlier sections, we derived expressions for the potential at some arbitrary position in a uniform TI medium, due to a current source on the surface. In this case, the Green's functions are simply evaluated as the potential divided by the current strength. In the case of the adjoint source (receiver position) we place a current source of strength I at this position and calculate the potential at the subsurface point in question. Obviously the co-ordinates specified for the true source to point P in the medium will be different to those for the adjoint source, although the functional form is identical.

Using the expression:

$$G = \frac{K}{R\left(1 + (\lambda^2 - 1)\cos^2\psi\right)^{1/2}} \tag{42}$$

with $K = \frac{\lambda\rho_l}{2\pi}$ we can calculate the derivatives needed using the chain rule as follows:

$$\begin{aligned}
\frac{\partial G}{\partial x} &= \frac{\partial G}{\partial \cos\psi} \cdot \frac{\partial \cos\psi}{\partial x} + \frac{\partial G}{\partial R} \cdot \frac{\partial R}{\partial x} \\
\frac{\partial G}{\partial y} &= \frac{\partial G}{\partial \cos\psi} \cdot \frac{\partial \cos\psi}{\partial y} + \frac{\partial G}{\partial R} \cdot \frac{\partial R}{\partial y} \\
\frac{\partial G}{\partial z} &= \frac{\partial G}{\partial \cos\psi} \cdot \frac{\partial \cos\psi}{\partial z} + \frac{\partial G}{\partial R} \cdot \frac{\partial R}{\partial z}
\end{aligned} \tag{43}$$

The various terms appearing in equation (43) can be evaluated thus:

$$\frac{\partial G}{\partial \cos\psi} = \frac{-K(\lambda^2 - 1).\cos\psi}{R(1 + (\lambda^2 - 1)\cos^2\psi)^{3/2}}, \tag{44}$$

$$\frac{\partial G}{\partial R} = \frac{-K}{R^2(1 + (\lambda^2 - 1)\cos^2\psi)^{1/2}}, \tag{45}$$

$$\frac{\partial R}{\partial x} = \frac{x}{R}, \quad \frac{\partial R}{\partial y} = \frac{y}{R}, \quad \frac{\partial R}{\partial z} = \frac{z}{R}. \tag{46}$$

The other derivatives of $\cos\psi$ with respect to x, y and z must also be obtained implicitly because of the x, y, and z dependence in the $\phi$ and $\theta$ terms which make up $\cos\psi$ (see equation 25):

$$\begin{aligned}
\frac{\partial \cos\psi}{\partial x} &= \frac{\partial \cos\psi}{\partial \phi} \cdot \frac{\partial \phi}{\partial x} + \frac{\partial \cos\psi}{\partial \theta} \cdot \frac{\partial \theta}{\partial x} \\
\frac{\partial \cos\psi}{\partial y} &= \frac{\partial \cos\psi}{\partial \phi} \cdot \frac{\partial \phi}{\partial y} + \frac{\partial \cos\psi}{\partial \theta} \cdot \frac{\partial \theta}{\partial y} \\
\frac{\partial \cos\psi}{\partial z} &= \frac{\partial \cos\psi}{\partial \phi} \cdot \frac{\partial \phi}{\partial z} + \frac{\partial \cos\psi}{\partial \theta} \cdot \frac{\partial \theta}{\partial z}
\end{aligned} \tag{47}$$

where

$$\frac{\partial \cos \psi}{\partial \phi} = -\sin \theta_0 \sin \theta \sin(\phi - \phi_0) = -\sin \theta_0 \sin \theta(\sin \phi \cos \phi_0 - \cos \phi \sin \phi_0)$$
$$\frac{\partial \cos \psi}{\partial \theta} = \sin \theta_0 \cos(\phi - \phi_0) \cos \theta - \cos \theta_0 \sin \theta \qquad (48)$$

The other derivatives for $\partial\theta/\partial x$, $\partial\theta/\partial y$, $\partial\theta/\partial z$, $\partial\phi/\partial x$, $\partial\phi/\partial y$, $\partial\phi/\partial z$ appearing in equation (47) are derived in the Appendix and shown to be:

$$\frac{\partial \theta}{\partial x} = \frac{xz}{R^2.(x^2 + y^2)^{1/2}}$$
$$\frac{\partial \theta}{\partial y} = \frac{yz}{R^2.(x^2 + y^2)^{1/2}} \qquad (49)$$
$$\frac{\partial \theta}{\partial z} = \frac{(x^2 + y^2)^{1/2}}{R^2}$$

and

$$\frac{\partial \phi}{\partial z} = 0,$$
$$\frac{\partial \phi}{\partial x} = -\frac{y}{x^2 + y^2},$$
$$\frac{\partial \phi}{\partial y} = \frac{1}{x.(1 + y^2/x^2)}. \qquad (50)$$

In the case of an isotropic medium $\lambda = 1$ and equation (44) is equal to zero. This yields all of the first set of terms on the right-hand side of equation (43) equal to zero, and therefore no dependence of the Fréchet derivatives on the polar angles: $\phi_0$, $\theta_0$. Equation (45) takes on the much simpler form: $-K/R^2$, independent of $\cos \psi$.

Returning to the anisotropic case, we have shown above that all of the required spatial derivatives of the Green's functions can be computed in terms of elementary functions involving the position coordinates $x$, $y$, $z$ for the subsurface point in question, be it measured from either the real current source or the adjoint current source.

It remains to calculate the various derivatives of the conductivity tensor with respect to the chosen parameters. In the TTI case this involves the following terms:

$$\frac{\partial \sigma_{xx}}{\partial \sigma_l}, \frac{\partial \sigma_{xx}}{\partial \sigma_t}, \frac{\partial \sigma_{xx}}{\partial \theta_0}, \frac{\partial \sigma_{xx}}{\partial \phi_0}$$
$$\frac{\partial \sigma_{yy}}{\partial \sigma_l}, \frac{\partial \sigma_{yy}}{\partial \sigma_t}, \frac{\partial \sigma_{yy}}{\partial \theta_0}, \frac{\partial \sigma_{yy}}{\partial \phi_0}$$
$$\frac{\partial \sigma_{zz}}{\partial \sigma_l}, \frac{\partial \sigma_{zz}}{\partial \sigma_t}, \frac{\partial \sigma_{zz}}{\partial \theta_0}, \frac{\partial \sigma_{zz}}{\partial \phi_0}$$

$$\frac{\partial \sigma_{xy}}{\partial \sigma_l}, \frac{\partial \sigma_{xy}}{\partial \sigma_t}, \frac{\partial \sigma_{xy}}{\partial \theta_0}, \frac{\partial \sigma_{xy}}{\partial \phi_0}$$

$$\frac{\partial \sigma_{xz}}{\partial \sigma_l}, \frac{\partial \sigma_{xz}}{\partial \sigma_t}, \frac{\partial \sigma_{xz}}{\partial \theta_0}, \frac{\partial \sigma_{xz}}{\partial \phi_0}.$$

$$\frac{\partial \sigma_{yz}}{\partial \sigma_l}, \frac{\partial \sigma_{yz}}{\partial \sigma_t}, \frac{\sigma_{yz}}{\partial \theta_0}, \frac{\partial \sigma_{yz}}{\partial \phi_0}$$

These derivatives are trivially simple and can be easily calculated from equation (16).

### 4.3. 2.5-D Case – Profile Perpendicular to Strike

We will now look at the special 2.5-D case in which the profile is assumed to be perpendicular to strike. Therefore the effect of azimuth can be ignored. In this situation we have $\sigma_{xy} = \sigma_{yz} = 0$ and all derivatives involving these components go to zero. Referring to equation (17) the only tensor derivative components to consider are:

$$\begin{aligned}
&\frac{\partial \sigma_{xx}}{\partial \sigma_l} = \cos^2 \theta_0, & &\frac{\partial \sigma_{xx}}{\partial \sigma_t} = \sin^2 \theta_0, \quad \frac{\partial \sigma_{xx}}{\partial \theta_0} = (-\sigma_l + \sigma_t) \sin 2\theta_0, \quad \frac{\partial \sigma_{xx}}{\partial \phi_0} = 0 \\
&\frac{\partial \sigma_{yy}}{\partial \sigma_l} = 1, & &\frac{\partial \sigma_{yy}}{\partial \sigma_t} = \frac{\partial \sigma_{yy}}{\partial \theta_0} = \frac{\partial \sigma_{yy}}{\partial \phi_0} = 0 \\
&\frac{\partial \sigma_{xz}}{\partial \sigma_l} = \frac{-\partial \sigma_{xz}}{\partial \sigma_t} = 0.5 \sin 2\theta_0, & &\frac{\partial \sigma_{xz}}{\partial \theta_0} = (-\sigma_l + \sigma_t) \cos 2\theta_0, & &\frac{\partial \sigma_{xz}}{\partial \phi_0} = 0 \\
&\frac{\partial \sigma_{zz}}{\partial \sigma_l} = \sin^2 \theta_0, & &\frac{\partial \sigma_{zz}}{\partial \sigma_t} = \cos^2 \theta_0, \quad \frac{\partial \sigma_{zz}}{\partial \theta_0} = (\sigma_l - \sigma_t) \sin 2\theta_0, \quad \frac{\partial \sigma_{zz}}{\partial \phi_0} = 0
\end{aligned} \tag{51}$$

Substituting into equation (39) we obtain the following expressions for the sensitivities:

$$\begin{aligned}
\frac{\partial U}{\partial \sigma_l} =& \cos^2 \theta_0 \frac{\partial G^A}{\partial x} \cdot \frac{\partial G^M}{\partial x} + \frac{\partial G^A}{\partial y} \cdot \frac{\partial G^M}{\partial y} + \sin^2 \theta_0 \cdot \frac{\partial G^A}{\partial z} \cdot \frac{\partial G^M}{\partial z} \\
&+ 0.5 \sin 2\theta_0 \left( \frac{\partial G^A}{\partial x} \cdot \frac{\partial G^M}{\partial z} + \frac{\partial G^A}{\partial z} \cdot \frac{\partial G^M}{\partial x} \right) \\
\frac{\partial U}{\partial \sigma_t} =& \sin^2 \theta_0 \frac{\partial G^A}{\partial x} \cdot \frac{\partial G^M}{\partial x} + \cos^2 \theta_0 \frac{\partial G^A}{\partial z} \cdot \frac{\partial G^M}{\partial z} - 0.5 \sin 2\theta_0 \left( \frac{\partial G^A}{\partial x} \cdot \frac{\partial G^M}{\partial z} + \frac{\partial G^A}{\partial z} \cdot \frac{\partial G^M}{\partial x} \right). \\
\frac{\partial U}{\partial \theta_0} =& (-\sigma_l + \sigma_t) \sin 2\theta_0 \frac{\partial G^A}{\partial x} \cdot \frac{\partial G^M}{\partial x} + (\sigma_l - \sigma_t) \sin 2\theta_0 \frac{\partial G^A}{\partial z} \cdot \frac{\partial G^M}{\partial z} \\
&+ (\sigma_l - \sigma_t) \cos 2\theta_0 \left( \frac{\partial G^A}{\partial x} \cdot \frac{\partial G^M}{\partial z} + \frac{\partial G^A}{\partial z} \cdot \frac{\partial G^M}{\partial x} \right)
\end{aligned} \tag{52}$$

In the isotropic case $(\sigma_l = \sigma_t = \sigma)$ we find that $\partial U / \partial \theta_0 = 0$, and the Fréchet derivative:

$$\frac{\partial U}{\partial \sigma} = \frac{1}{2}\left(\frac{\partial U}{\partial \sigma_l} + \frac{\partial U}{\partial \sigma_t}\right),$$

leads to a cancellation of all the cross terms involving the Green's functions and elimination of all $\theta_0$ dependence, yielding the same result as equation (41). Note that $\partial U/\partial \rho = -\frac{1}{\rho^2}\partial U/\partial \sigma$, yielding a scaling factor and change of sign between the conductivity and resistivity sensitivities.

## 5. Illustrative Examples

The equations derived earlier were incorporated into a simple computer program to calculate the potential, current density and Fréchet derivatives (for a pole-pole array) at any interior point within a uniform TTI medium of arbitrary dip, strike, average conductivity and coefficient of anisotropy. Figure 6a shows the equipotential and current density patterns in the subsurface for a surface current electrode over a uniform, isotropic medium with a conductivity of 0.1 S/m. The diagram is for a single vertical slice through the current electrode which is located at position (0, 0). Note the circular equipotential patterns and the constant magnitude of the current density vectors (indicated by arrows) at a fixed radial distance from the current electrode. There is no angular variation of the current density. Both the potential and the current density fall off inversely with distance. Note also that the current density vectors are everywhere orthogonal to the equipotential contours. By contrast, Figure 6b shows the corresponding patterns for a current electrode on the surface above a uniform, anisotropic TI medium with a longitudinal conductivity of 0.1 S/m, a transverse conductivity of 0.02 S/m (coefficient of anisotropy of 2.2) and a dipping axis of symmetry of tilt angle 45 degrees. The azimuth of the axis of symmetry is $\phi_0 = 0°$. The cross section is at an azimuth of $\phi = 0°$ and passes through the current source. We now observe a pronounced asymmetry in the equipotential patterns (elliptical) with the long axis of the ellipse in the longitudinal direction (i.e., parallel to the bedding plane). The current density now not only falls off with increasing distance from the current source but there is also a pronounced angular variation, with maximum current density in the longitudinal (most conductive) direction (i.e., parallel to the plane of stratification) and minimum current density in the transverse conductivity direction (parallel to the bedding plane normal). Also we observe that the current density vectors are no longer perpendicular to the equipotential contours, except along the axes of the ellipse.

We now wish to examine the Fréchet derivatives. First we show in Figure 7 the sensitivity pattern *dG/dσ* for an isotropic medium in which the conductivity is 0.1 S/m. The current source is at position (5, 0) and the potential electrode at position (10,0). The cross section shown passes through the electrodes and is at an azimuth of 0°. The pattern is symmetrical, with maxima close to the electrodes. The sensitivities are positive between the electrodes and negative on either side (the opposite pattern would be obtained if we plotted *dG/dρ*). This isotropic sensitivity plot is identical to that obtained by other authors
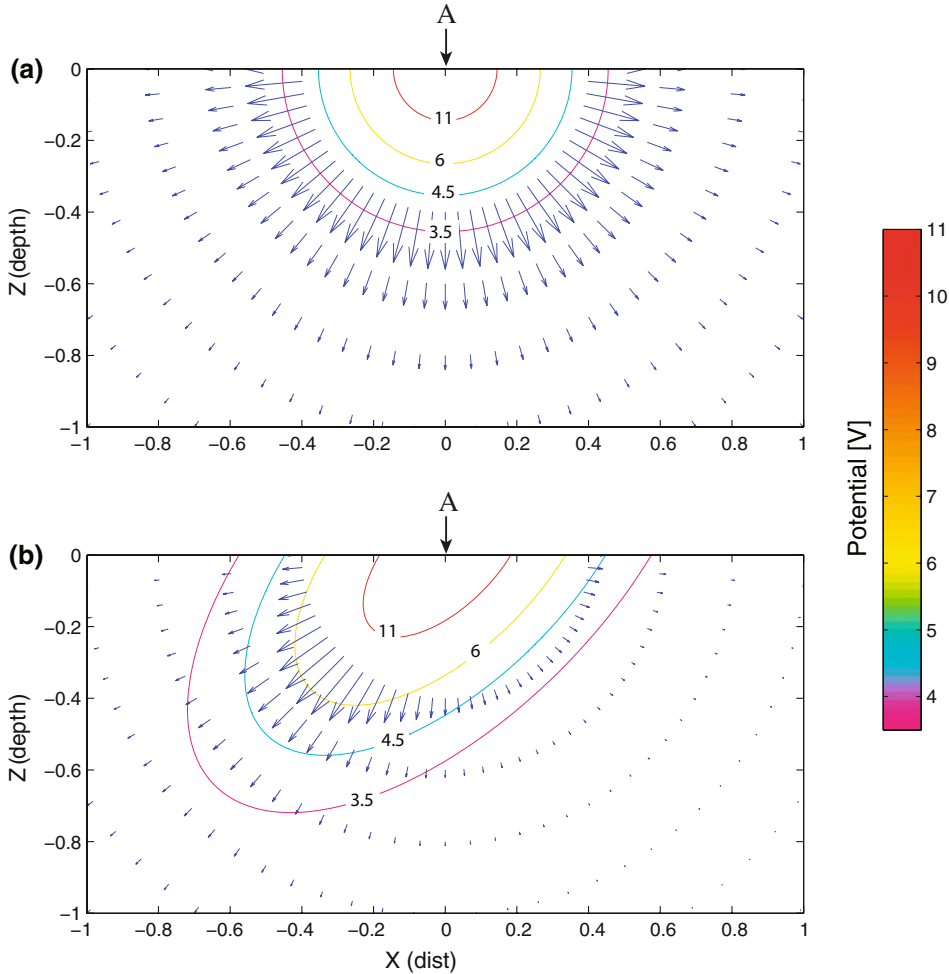
Figure 6

The equipotential contours and current density vectors (shown by arrows) for (a) an isotropic medium of conductivity 0.1 S/m, and (b) an anisotropic medium with a longitudinal conductivity of 0.1 S/m, a transverse conductivity of 0.025 S/m, and a dip angle for the axis of symmetry of 45 degrees. The profile is perpendicular to the strike. Note how the current density vectors vary with the angle in the anisotropic case, being maximum parallel to the plane of stratification (longitudinal direction), and are not perpendicular to the equipotential contours.

(e.g., SPITZER, 1998). We now wish to contrast the isotropic pattern with that for an anisotropic medium having a coefficient of anisotropy of $\lambda = 2$ ($\sigma_l = 0.1 S/m$, $\sigma_t = 0.025 S/m$). Again the cross-sections shown will be for an azimuth $\phi = 0°$ (i.e., perpendicular to strike of the plane of stratification) and passing through the electrodes. The current electrode is at position (5, 0) and the potential electrode is at (10, 0), as for the isotropic case (Fig. 7). Three different derivatives must be considered in the anisotropic
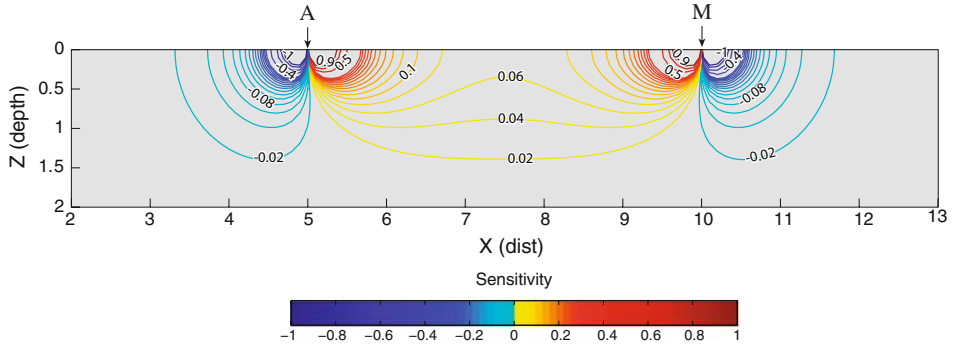
Figure 7

Fréchet derivatives $dG/d\sigma$ in the subsurface for a uniform isotropic medium ($\sigma = 0.1$ S/m) with the current electrode at (5, 0) and the potential electrode at (10, 0). Note the symmetry of the pattern, maxima around the electrodes and reversal of sign.

case: $dG/d\sigma_l$, $dG/d\sigma_t$, $dG/d\theta_0$. Results are given in Figures 8, 9 and 10, respectively. Each figure shows the sensitivity patterns for three different values of the dip of the symmetry axis, $\theta_0 = 15, 45, 75$ degrees. Unlike the isotropic case, the anisotropic sensitivity patterns are all distinctly asymmetrical. The longitudinal conductivity sensitivity $\partial G/d\sigma_l$ contours of greatest magnitude (Fig. 8) are aligned and elongated in the direction of lines that run from the electrodes parallel to the plane of isotropy (i.e., orthogonal to the axis of symmetry). Conversely, the smallest sensitivity regions are found along lines that run from the electrodes parallel to the axis of symmetry. In comparison to the isotropic pattern (Fig. 7), all plots exhibit shifts in the positions of both the negative and positive contours such that they follow the direction of maximum conductivity. The sensitivities decrease markedly with increasing dip. There is negligible longitudinal conductivity sensitivity at the surface between and outside the electrodes for the $\theta_0 = 75°$ case (corresponding to steeply dipping beds).The transverse conductivity sensitivities $\partial G/d\sigma_t$, shown in Figure 9, again display an asymmetrical pattern, with the greatest magnitude sensitivity along lines drawn through the electrodes that are orthogonal to the plane of isotropy (i.e., parallel to the axis of symmetry). Sensitivity is smallest in magnitude along lines drawn through the electrodes which are parallel to the plane of isotropy, i.e., in the minimum conductivity direction. This is in striking contrast to the longitudinal sensitivity pattern (Fig. 8). The steepness of the pattern increases with increasing dip angle $\theta_0$, and by comparison with the corresponding $dG/d\sigma_l$ pattern, there is appreciable sensitivity both at the surface and in the subsurface for all dips. In fact, there is greater sensitivity at depth with increasing dip. The sensitivities are mainly positive between the electrodes but actually become negative at a depth of half the electrode separation in the case of shallow dip ($\theta_0 = 15°$). The sensitivity pattern $dG/d\theta_0$, shown in Figure 10, exhibits a rather unusual pattern. For small dips (15°) the plot is dominated by the region below the electrodes, with the null lines elongated parallel to the plane of isotropy. For intermediate (45°) and steep dips (75°) the plots look remarkably similar to the $dG/d\sigma_l$ patterns, with large magnitude sensitivities
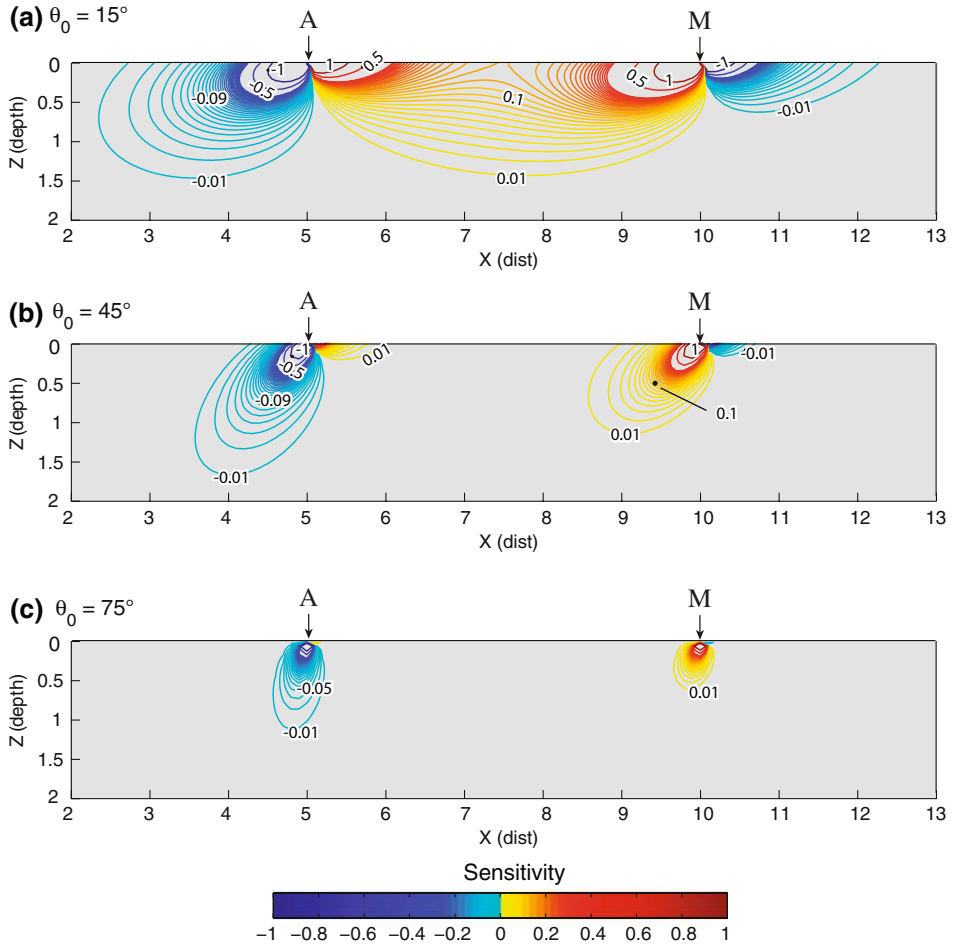
**Figure 8**

Fréchet derivatives for the longitudinal conductivity, $dG/d\sigma_l$, in an anisotropic TTI medium which has longitudinal conductivity 0.1 S/m, and transverse conductivity 0.025 S/m (coefficient of anisotropy $\lambda = 2$). The profile is perpendicular to the strike. Results are given for three different dips of the symmetry axis (transverse resistivity direction): 15° (a), 45° (b) and 75° (c) degrees down to the right. Note the strong asymmetry of the pattern compared to Figure 7 and the elongation of contours in the direction of the plane of stratification (longitudinal conductivity direction).

areas located along lines drawn through the electrodes and in the direction perpendicular to the axis of symmetry. However, sensitivity drops dramatically between the electrodes as the dip increases.

The validity of the plots has been confirmed by comparison with results obtained numerically. Of course, the analytic plots are much "cleaner" and do not suffer from numerical artefacts. The Fréchet derivatives in heterogeneous, anisotropic media are the subject of ongoing research. The analytic solution reported here serves not only as a
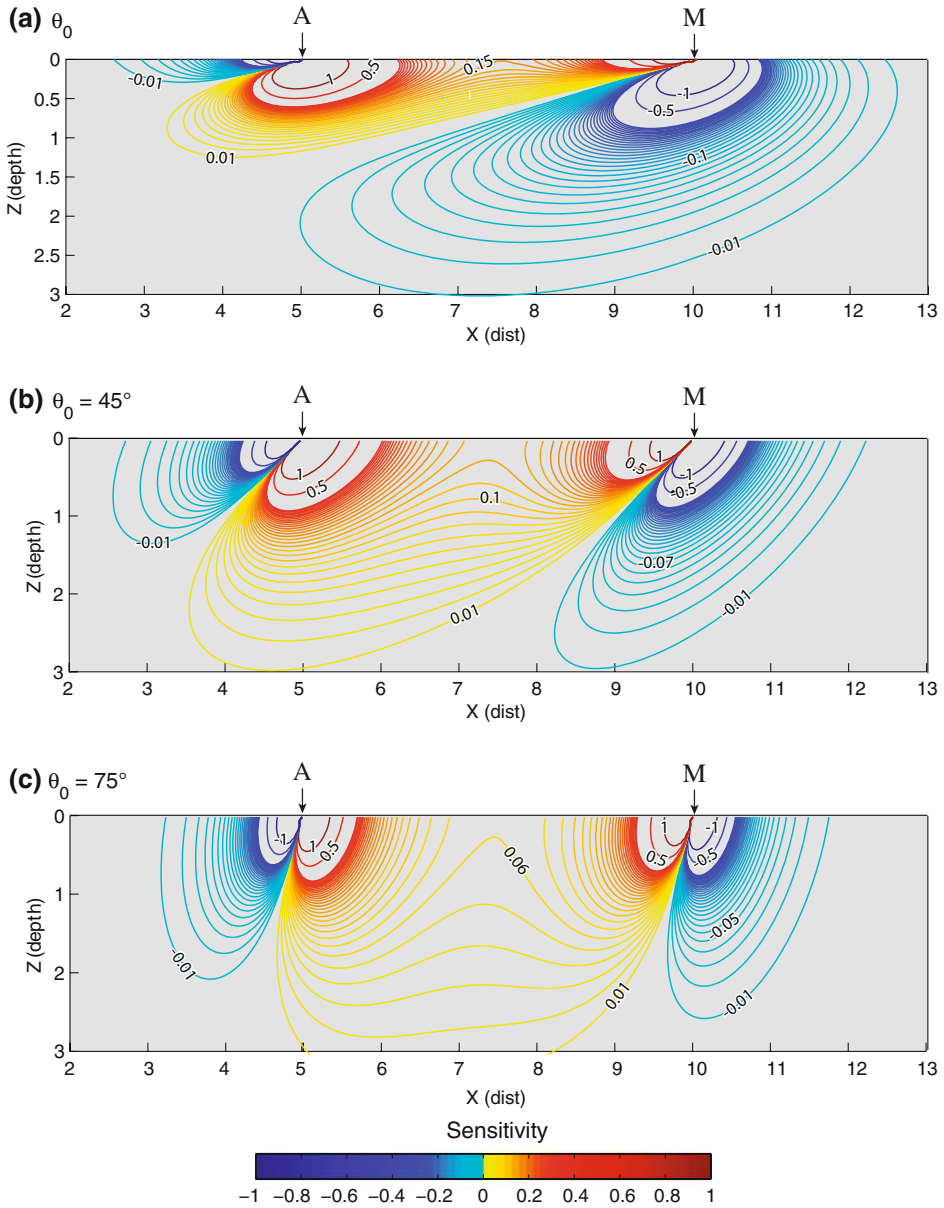
Figure 9

Fréchet derivatives for the transverse conductivity, $dG/d\sigma_t$. The same anisotropic TTI model and electrode configuration (pole-pole) are derived as in Figure 8. The three cross sections are for different dips of the symmetry axis: 15° (a), 45° (b) and 75° (c). Again strong asymmetry in the patterns exists, with maxima around the electrodes and a decrease in sensitivity with depth.
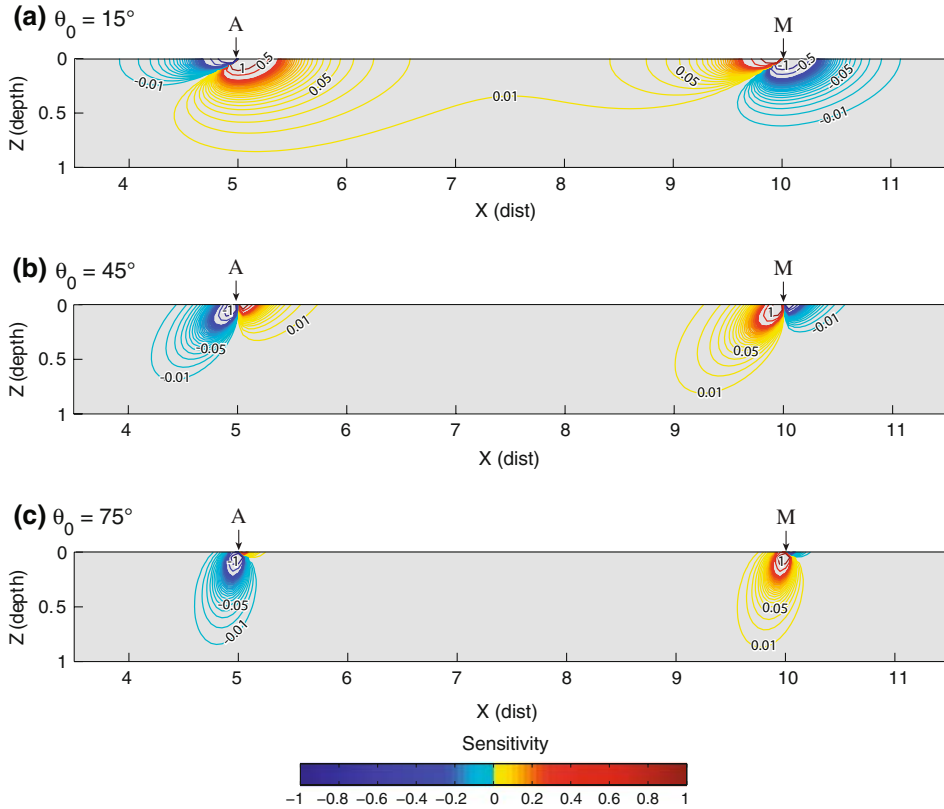
Figure 10

Fréchet derivatives for the dip angle of the symmetry axis, $dG/d\theta_0$. The same anisotropic TTI model and electrode configuration are derived as for Figures 8 and 9. The three cross sections are for different dips of the symmetry axis: 15° (a), 45° (b) and 75° (c). Note how the patterns become increasingly asymmetric with increasing dip.

benchmark for assessing the accuracy of the numerical solutions but also allows one to illuminate the behaviour of DC fields and sensitivity patterns present in 3-D numerical computations but often obscured by excessive complexity. In companion papers (GREENHALGH *et al.*, 2008b; WIESE *et al.*, 2008), we have undertaken a comprehensive analysis of the complete set of Fréchet derivatives, expressed in terms of principal values (or alternative $\sigma_m$, $\lambda$ formulation) and polar angles of the symmetry axis, for a wide range of dips, azimuths and anisotropy ($\lambda$) values. These other studies illustrate the dangers of using isotropic sensitivities when the ground is anisotropic, the consequences of electrical equivalence, and also some rather peculiar zero sensitivity conditions. In terms of experimental design, it seems mandatory to incorporate downhole electrodes to discriminate and characterise anisotropy. Although field determinations of anisotropy are beyond the scope of this article, it is insufficient to rely on surface measurement procedures such as azimuthal resistivity surveys (BUSBY, 2000) and square array techniques (MATIA, 2002) alone.

## 6. Conclusions

We have reviewed the basic properties of the electric conductivity tensor and the tensor ellipsoid. Equations are developed for computing the six individual components of the tensor in terms of the principal conductivities and the angles defining the major symmetry axis. For an anisotropic medium the current density vector is not perpendicular to the equipotentials but is perpendicular to the tangent plane at to the surface of the ellipsoid for a given direction of the electric field. We have derived the basic equations for the electric potential, current density and Fréchet derivatives at any interior point within a uniform anisotropic model. The model we consider is a tilted transversely isotropic solid characterised by four parameters: longitudinal conductivity $\sigma_l$, transverse conductivity $\sigma_t$, strike of the symmetry axis $\phi_0$ and dip of the symmetry axis $\theta_0$. Representative plots are given showing the sensitivity variations (Fréchet derivatives) for different combinations of the parameters. In contrast to the isotropic case, there is pronounced asymmetry in the Fréchet derivative patterns, which show an alignment with the plane of stratification. Knowledge of the derivatives will be useful in designing 3-D surface electrode arrays (tensor field measurements) to best recover anisotropy, and in the inversion of actual resistivity data. This is the subject of ongoing research, however results to date show some rather surprising patterns and the need to incorporate downhole electrodes to detect and characterise electrical anisotropy

## *Appendix. Derivation of the $\theta$ and $\phi$ Spatial Derivatives*

Equation (47) involves spatial derivatives terms of the polar angles $\theta$ and $\phi$ which specify, along with radial distance R, the subsurface point $(x, y, z)$ at which the Fréchet derivative is to be computed. Here we derive equations for these derivatives.

For the $\theta$ derivatives we use the relation:

$$\cos\theta = z/R = z/(x^2 + y^2 + z^2)^{1/2} \tag{A1}$$

to obtain

$$
\begin{aligned}
-\sin\theta \frac{\partial\theta}{\partial x} &= \frac{\partial}{\partial x}\left(\frac{z}{(x^2+y^2+z^2)^{1/2}}\right) = \frac{-xz}{(x^2+y^2+z^2)^{3/2}} \\
-\sin\theta \frac{\partial\theta}{\partial y} &= \frac{-yz}{(x^2+y^2+z^2)^{3/2}} \\
-\sin\theta \frac{\partial\theta}{\partial z} &= \frac{\partial}{\partial z}\left(\frac{z}{(x^2+y^2+z^2)^{1/2}}\right) = \frac{x^2+y^2}{(x^2+y^2+z^2)^{3/2}}
\end{aligned}
\tag{A2}
$$

But

$$\sin \theta = (1 - \cos^2 \theta)^{1/2} = (1 - z^2/R^2)^{1/2} = (x^2 + y^2)^{1/2}/R. \qquad \text{(A3)}$$

This then yields for the $\theta$ derivatives:

$$\frac{\partial \theta}{\partial x} = \frac{xz}{R^2.(x^2 + y^2)^{1/2}}$$

$$\frac{\partial \theta}{\partial y} = \frac{yz}{R^2.(x^2 + y^2)^{1/2}}.$$

$$\frac{\partial \theta}{\partial z} = \frac{(x^2 + y^2)^{1/2}}{R^2}$$

For the $\phi$ derivatives we use the relation

$$\tan \phi = y/x \qquad \text{(A4)}$$

to obtain

$$\frac{\partial \phi}{\partial z} = 0$$

$$\sec^2 \phi.\frac{\partial \phi}{\partial x} = \frac{-y}{x^2}, \quad \sec^2 \phi.\frac{\partial \phi}{\partial y} = \frac{1}{x} \qquad \text{(A5)}$$

with

$$\sec^2 \phi = 1 + \tan^2 \phi = 1 + (y^2/x^2) \qquad \text{(A6)}$$

giving

$$\frac{\partial \phi}{\partial x} = -\frac{y}{x^2 + y^2}$$
$$\frac{\partial \phi}{\partial y} = \frac{1}{x.(1 + y^2/x^2)} \qquad \text{(A7)}$$

## REFERENCES

ASTEN, M.W. (1974), *The influence of electrical anisotropy on mise-a-la masse surveys,* Geophys. Prosp. *22*, 238–245.

BHATTACHARYA, P.K. and PATRA, H.P., *Direct Current Geoelectric Sounding: Principles and Applications* (Elsevier, Amsterdam 1968).

BUSBY, J.P. (2000), *The effectiveness of azimuthal apparent resistivity measurements as a method for determining fracture strike orientations*, Geophys. Prosp. *48*, 677–698.

DAS (1995)

ELORANTA, E.H. (1988), *The modelling of mise-a-la masse anomalies in an anisotropic half space by the integral equation method*, Geoexploration *25*, 93–101.

Eskola, L. and Hongisto, H (1997), *Resistivity and IP modelling of an anisotropic body located in an isotropic environment*, Geophys. Prosp. *45*, 127–139.

Flykt, M.J., Eloranta, E.H., Nikoskinen, K.I., Lindell, I.V. and Sihvola, A.H. (1996), *DC potential anomalies caused by a conducting body in an anisotropic conducting half space*, IEEE Trans. Geosci. Remote Sens. *34*, 27–32.

Greenhalgh, S.A., Zhou, B., Greenhalgh, M., and Marescot, L. (2008a), *Explicit expressions for the Fréchet derivatives in 3-D anisotropic resistivity inversion*, Geophys. (in press).

Greenhalgh, S.A., Wiese, T., and Marescot, L. (2008b), *Comparison of anisotropic and isotropic DC sensitivity patterns*, J. Applied Geophys. (submitted).

Herwanger, J.V., Pain, C.C, Binley, A., de Olivereira, C.R.E., and Worthington, M.H. (2004), *Anisotropic resistivity tomography*, Geophys. J. Int. *158*, 409–425.

Keller, G.V. and Frischknecht, F.C., *Electrical Methods in Geophysical Prospecting* (Pergamon Press, Oxford 1970).

Kim, J., Yi, M., Cho, S., Son, J., and Song, W. (2006), *Anisotropic crosshole resistivity tomography for ground safety analysis of a high-storied building over an abandoned mine*, J. Envir. Eng. Geophys. *11*, 225–235.

Li, P. and Uren, N.F. (1997), *The modelling of direct current electric potential in arbitarily anisotropic half-space containing a conductive body*, J. Applied Geophys. *38*, 57–76.

Li, P. and Uren, N. (1998), *Analytical solution for the electric potential due to a point source in an arbitrary anisotropic half space*, J. Eng. Math. *33*, 129–140.

Li, P. and Stagnitti, F. (2000), *Direct current electric potential in an anisotropic half space with vertical contact containing a conductive 3-D body*, Math. Eng. *1*, 63–77.

Li, Y. and Spitzer, K. (2005), *Finite element resistivity modelling for three-dimensional structures with arbitrary anisotropy*, Phys. Earth Plan. Int. *150*, 15–27.

Loke, M.H. and Barker, R.D. (1995), *Least-squares deconvolution of apparent resistivity pseudosections*, Geophysics *60*, 1682–1690.

Maillet, R. (1947), *The fundamental equations of resistivity prospecting*, Geophys. *12*, 529–556.

Matia, M.J. (2002), *Square array anisotropy measurements and resistivity sounding interpretation*, J. Appl. Geophys. *49*, 185–194.

Nye, J.F., *Physical Properties of Crystals* (Oxford University Press, Oxford 1957).

Pal, B.P. and Dasgupta, S.P. (1984), *Electrical potential due to a point current source over an inhomogeneous anisotropic earth*, Geophys. Prosp. *32*, 943–954.

Pal, B.P. and Mukherjee, K. (1986), *Electrical potential due to a point current source over a layered conducting earth with dipping anisotropy*, Geoexploration *24*, 15–19.

Pain, C., Herwanger, J., Saunders, J., Worthington, M., and Oliveira, C. (2003), *Anisotropic resistivity inversion*, Inverse Problems *19*, 1081–1111.

Pervago, E., Ousatov, A., and Shevnin, V. (2006), *Analytic solution for the electric potential in arbitrary anisotropic layered media applying the set of Hankel transforms of integer order*, Geophys. Prosp. *54*, 651–661.

Spitzer, K. (1998), *The three-dimensional DC sensitivity for surface and subsurface sources*, Geophys. J. Int. *134*, 736–746.

Stummer, P., Maurer, H.R., and Green, A.G. (2004), *Experimental design: electrical resistivity data sets that provide optimal subsurface information*, Geophys. *69*, 120–139.

Wait, J.R., *Geoelectromagnetism*, (Academic Press, San Diego 1982).

Wait, J.R. (1990), *Current flow into a three-dimensionally anisotropic conductor*, Radio Science *25*, 689–694.

Wiese, T., Greenhalgh, S.A., and Marescot, L. (2009), *DC sensitivity patterns for tilted transversely isotropic media*, Near Surface Geophys. 123–127.

Yin, C. and Wiedelt, P. (1999), *Geoelectrical fields in layered earth with arbitrary anisotropy*, Geophys. *64*, 426–434.

Zhou, B. and Greenhalgh, S.A. (1999), *Explicit expressions and numerical computation of the Frechet and second derivatives in 2.5D Helmholtz equation inversion*, Geophys. Prosp. *47*, 443–468.

Zhou, B. and Greenhalgh, S.A. (2002), *Rapid 2-D/3-D crosshole resistivity imaging using the analytic sensitivity function*, Geophys. *67*, 755–765.

ZHOU, B. and GREENHALGH, S.A. (2004), *On the computation of elastic wave group velocities for a general anisotropic medium*, J. Geophys. Eng. *1*, 205–215.

ZHOU, B., GREENHALGH, M., and GREENHALGH, S.A. (2009), *2-D/3-D electrical resistivity modelling in heterogeneous anisotropic media using Gaussian quadrature grids*, Geophys. Journal Int. (in press).

To access this journal online:
www.birkhauser.ch/pageoph